13

Destruction of Fluorinated Greenhouse Gases by Using Nonthermal Plasma Process

Young Sun Mok
Department of Chemical & Biological Engineering, Jeju National University
Republic of Korea

1. Introduction

Most of fluorinated compounds such as hydrofluorocarbons (HFCs), perfluorocarbons (PFCs) and sulfur hexafluoride (SF_6) are considered as significant greenhouse gases due to their chemical stability, long atmospheric lifetimes, and high infrared absorption capacity. The 100-year global warming potentials (GWPs) of them are reported to be from a few thousand times to tens of thousand times that of carbon dioxide (CO_2). Fluorinated compounds have been widely used in semiconductor and polymer industries, commercial refrigeration and air conditioning. SF_6 that is the most potent greenhouse gas with a GWP of 22,200 has been used as a common gaseous dielectric medium in electrical power equipments and in the etching and cleaning processes of the semiconductor industry. Up to now, several technologies for abating such gaseous fluorinated compounds have been developed, which include incineration, catalytic decomposition, thermal or nonthermal plasma destruction, and so forth (Bickle et al., 1994; Futamura & Yamamoto, 1997; Lee & Choi, 2004; Ogata et al., 2004; Föglein et al., 2005; Mizeraczyk et al., 2005). Even though the incineration is the only field-proven technology so far, it necessarily requires a lot of energy and long preheating time to reach high temperature enough to destroy chemical bonds in fluorinated compounds. The use of catalyst can largely lower the operation temperature, but still high temperature above 700°C is needed to achieve sufficient catalytic activity. The application of thermal or nonthermal plasma to the destruction of fluorinated compounds as an emission control technology is a relatively new research area. Previous studies have shown that low-pressure plasma processes like inductively coupled plasma (ICP) can destroy fluorinated compounds effectively (Kuroki et al., 2005). However, they inevitably require high investment and operation cost for vacuum. For this reason, atmospheric nonthermal plasma systems can be more desirable from a practical point of view.

The non-thermal plasma has been created in different plasma reactors such as microwave, pulsed streamer corona and dielectric barrier discharge (DBD) reactors, offering an innovative approach for the abatement of fluorinated compounds. The pulsed corona discharge is induced by the application of fast-rising narrow high voltage pulse to non-uniform electrode geometry (Mok et al., 1998). It develops by forming a number of streamers, the starting points of which are discrete and distributed over the surface of discharging electrode. Free electrons produced by the discharge can be accelerated by an imposed electric field to gain energy. During their drift, they can collide with various molecules and lose energy. The collisions of energetic electrons with gas molecules result in the formation of various reactive species. The DBD is a kind of gaseous electrical discharge

occurring between two electrodes separated by at least one insulating layer. Typically, DBD reactors use high voltage alternating current (AC) and operate in atmospheric pressure range. The DBD plasma reactor becomes increasingly very attractive due to its capability of producing abundant reactive species by enormous energetic electron collisions with running gas molecules at atmospheric pressure. In addition, dielectric barrier discharge plasma reactors are generally compact and operates stably with high average power.

The drawbacks associated with the nonthermal plasma destruction of fluorinated compounds may be high energy consumption, slow destruction rate and unwanted byproducts formation. In order to get over these problems, recent studies have been focused on the combination of plasma with catalysis (Kim et al., 2005). The use of catalysis together with nonthermal plasma can promote the oxidative destruction of fluorinated compounds through C-F bond cleavage and prevent the recombination of decomposed fragments, thereby remarkably depressing unwanted byproducts formation. As well, the nonthermal plasma can assist catalytic reactions by triggering additional activation of catalyst. As demonstrated in many studies conducted elsewhere, the combination of nonthermal plasma and catalysis has provided a broad range of applications.

In this work, the destruction of fluorinated compounds, including trifluoromethane (CHF_3 or HFC-23), sulfur hexafluoride (SF_6), 1,1,1,2-tetrafluoroethane ($C_2H_2F_4$ or HFC-134a) and hexafluoroethane (C_2F_6), has been investigated over a wide temperature range up to 500°C with a dielectric-packed nonthermal plasma reactor and a simulated exhaust gas consisting of fluorinated compounds, oxygen and nitrogen. The GWP values and atmospheric lifetimes of these greenhouse gases are summarized in Table 1 (Intergovernment Panel on Climate Change Third Assessment Report, 2011).

Chemcial formula	Code name	GWP (-)	Atmospheric lifetime (yr)
CHF_3	HFC-23 or R-23	12,000	260
$C_2H_2F_4$	HFC-134a or R-134a	1,300	13.8
SF_6	-	22,200	3,200
C_2F_6	R-116	11,900	10,000

Table 1. Global warming potentials and atmospheric lifetimes of fluorinated compounds

The nonthermal plasma can be used not only to produce a variety of reactive species capable of destroying gaseous pollutants, but also to improve catalytic activity through various actions. In this context, proper selection of a packing material that can in turn affect the performance of the plasma reactor is of great importance. There have been several previous articles of our research group, where the characteristics of three different packing materials such as alumina, zirconia and glass beads were comparatively examined (Kim et al., 2010a, 2010b; 2010c; Kim & Mok, 2011a). In those articles, the destruction behaviors of the fluorinated compounds were characterized with respect to electric power and reactor temperature, and the effects of several other variables on the destruction were evaluated. In this paper, various aspects of the nonthermal plasma destruction of fluorinated compounds were discussed and plausible destruction mechanisms were illustrated with experimental results, referring to the previous articles of our research group. Two key parameters controlling the performance are the electric power and the reactor temperature, because they dominate reactive species generation and catalytic reaction rate, respectively.

2. Theoretical background

Electrical discharge plasma - that is the DBD plasma - produces various reactive spcies including excited molecules (ex. N_2 ($A^3\Sigma_u^+$)), excited atoms (ex. O(^{1}D) and N(^{2}D)), radicals (ex. OH and HO_2), ions and energetic electrons, all of which can contribute to the destruction of gaseous pollutants more or less. When it comes to the destruction of fluorinated compounds with strong carbon-fluorine bond, however, the reactive species that are mainly responsible for the destruction are considered to be excited atoms, radicals and energetic electrons rather than excited molecules and ions. The destruction mechanisms of the fluorinated compounds dealt with in this work are elucidated below.

2.1 Basic processes

High-energy electrons, i.e., energetic electrons created by nonthermal electrical discharge plasma are in the range of 5~10 eV (1 eV = 1.6×10^{-19} J) on the average. The production of reactive species associated with the destruction of fluorinated compounds is initiated by collisions between energetic electrons and background molecules like H_2O, N_2 and O_2. The electron-molecule collision processes are

$$e + N_2 \rightarrow e + N_2(A^3\Sigma_u^+) \tag{1}$$

$$e + N_2 \rightarrow e + N + N \tag{2}$$

$$e + O_2 \rightarrow e + O + O \tag{3}$$

$$e + O_2 \rightarrow e + O + O\left(^1D\right) \tag{4}$$

$$e + H_2O \rightarrow e + H + OH \tag{5}$$

The rates of reactions (1)-(5) are a function of electron energy, namely, imposed electric field, which can be estimated from the solution of Boltzmann equation and the appropriate collision cross-section data. The excited atomic oxygen O(^{1}D) generated from reaction (4) can produce additional OH radicals as a result of rapid quenching with H_2O as follows:

$$O\left(^1D\right) + H_2O \rightarrow OH + OH \tag{6}$$

The rate constant for reaction (6) is reported to be 2.6×10^{-10} cm^3 $molecule^{-1}$ (Li et al., 1995; Chang et al., 1991). In the case of electron-beam irradiation process utilizing fast electrons in the range of 300~750 keV, most of OH radicals are formed through charge-exchange reactions. On the other hand, the OH formation by nonthermal plasma is dominated by hydrogen abstraction from water vapor by O(^{1}D) under most conditions.

2.2 Destruction pathways

2.2.1 Trifluoromethane

In most cases, the major constituent of contaminated gas to be treated is nitrogen. Regarding the reaction of excited state N_2 ($A^3\Sigma_u^+$) with CHF_3, Piper et al. (1985) identified the process as

$$N_2(A^3\Sigma_u^+,\ v=1)\ +\ CHF_3 \rightarrow N_2(A^3\Sigma_u^+,\ v=0)\ +\ CHF_3\ \ 6.0\times10^{11}\,cm^3mol^{-1}s^{-1} \qquad (7)$$

Tao et al. (1992) also reported the dominant process to be vibrational relaxation. Thus, it is reasonable to consider the CHF_3 destruction by excited state $N_2(A^3\Sigma_u^+)$ to be negligible. On the contrary, electronically excited atomic nitrogen $N(^2D)$ can play an important role in destroying CHF_3 by abstracting hydrogen atom (Herron, 1999)

$$N\left(^2D\right) + CHF_3 \rightarrow NH + CF_3,\ 6.0\times10^{10}\,cm^3mol^{-1}s^{-1} \qquad (8)$$

The rate coefficients of reactions (7) and (8) are the values at 298 K, and other rate coefficients given below are also at 298 K. Energetic electrons can also initiate the destruction of CHF_3. The destruction products formed by the energetic electrons may be inferred by referring to mass spectroscopy, since the electron impact dissociation has some analogy with fragmentation reactions in a mass spectrometer. The cracking pattern of CHF_3 indicates that the most abundant destruction products are CF_3 and CHF_2. Thus, the electron impact dissociations can be written as

$$e + CHF_3 \rightarrow CF_3 + H + e \qquad (9)$$

$$e + CHF_3 \rightarrow CHF_2 + F + e \qquad (10)$$

The bond dissociation energies of C-H and C-F are 4.3 and 5.1 eV, respectively. Although C-F has larger bond energy than C-H, strong electro-negativity of F atom can lead to reaction (10). Both reactions (9) and (10) depend on the electric field controlling the electron energy. H and F radicals from reactions (9) and (10) can react as follows (Barker, 1995; NIST, 1998):

$$H + CHF_3 \rightarrow H_2 + CF_3, \qquad 2.2\times10^4\,cm^3mol^{-1}s^{-1} \qquad (11)$$

$$F + CHF_3 \rightarrow HF + CF_3, \qquad 9.4\times10^{10}\,cm^3mol^{-1}s^{-1} \qquad (12)$$

The small rate coefficient of reaction (11) implies that the contribution of H radical to the CHF_3 destruction is insignificant. In the presence of oxygen, reactions (3)~(6) form O and OH radicals, which participate in the following reactions (Barker, 1995; NIST, 1998)

$$O + CHF_3 \rightarrow OH + CF_3, \qquad 7.6\times10^4\,cm^3mol^{-1}s^{-1} \qquad (13)$$

$$OH + CHF_3 \rightarrow H_2O + CF_3,\ 2.9\times10^8\,cm^3mol^{-1}s^{-1} \qquad (14)$$

Compared to reactions (8), (12) and (14), the rate of reaction (13) is much slower, implying that the contribution of atomic oxygen to the destruction is trivial.

The processes for the primary destruction steps (reactions (8)~(14)) produce CF_3 and CHF_2, which can react with oxygen to form peroxy radicals

$$CF_3 + O_2 \rightarrow CF_3O_2, \qquad 2.4\times10^{12}\,cm^3mol^{-1}s^{-1} \qquad (15)$$

$$CHF_2 + O_2 \rightarrow CHF_2O_2, \quad 2.4\times10^{12}\,cm^3mol^{-1}s^{-1} \qquad (16)$$

where the rate coefficient for reaction (16) was assumed to be equal to that for reaction (15) (Barker, 1995). The peroxy radicals, i.e., CF_3O_2 and CHF_2O_2, further react to form alkoxy radicals as (Barker, 1995; NIST, 1998)

$$CF_3O_2 + CF_3O_2 \rightarrow 2CF_3O + O_2, \quad 1.36\times10^{12}\,\mathrm{mol^{-1}s^{-1}} \tag{17}$$

$$CHF_2O_2 + CHF_2O_2 \rightarrow 2CHF_2O + O_2, \quad 3.0\times10^{12}\,\mathrm{mol^{-1}s^{-1}} \tag{18}$$

$$CF_3O_2 + NO \rightarrow CF_3O + NO_2, \quad 9.6\times10^{12}\,\mathrm{mol^{-1}s^{-1}} \tag{19}$$

$$CHF_2O_2 + NO \rightarrow CHF_2O + NO_2, \quad 7.8\times10^{12}\,\mathrm{mol^{-1}s^{-1}} \tag{20}$$

It should be noted that NO involved in reactions (19) and (20) is formed by the reaction between excited atomic nitrogen $N(^2D)$ and O_2 (Ricketts et al., 2004; Harling et al., 2005). The alkoxy radicals CF_3O and CHF_2O formed by the reactions (17)~(20) are further degraded to give carbonyl fluoride (COF_2) as follows (Barker, 1995; NIST, 1998):

$$CF_3O + O_2 \rightarrow COF_2 + FO_2, \quad 1.0\times10^{6}\,\mathrm{mol^{-1}s^{-1}} \tag{21}$$

$$CHF_2O + O_2 \rightarrow COF_2 + HO_2, \quad 1.1\times10^{9}\,\mathrm{cm^3mol^{-1}s^{-1}} \tag{22}$$

$$CF_3O + CO \rightarrow COF_2 + COF, \quad 1.2\times10^{9}\,\mathrm{cm^3mol^{-1}s^{-1}} \tag{23}$$

$$CF_3O + NO \rightarrow COF_2 + NOF, \quad 3.2\times10^{13}\,\mathrm{cm^3mol^{-1}s^{-1}} \tag{24}$$

$$CF_3O + NO_2 \rightarrow COF_2 + NO_2F, \quad 1.9\times10^{12}\,\mathrm{cm^3mol^{-1}s^{-1}} \tag{25}$$

Although the rate coefficient of reaction (21) is small, its reaction rate is not negligible because oxygen is often one of the main constituents in the gas to be treated. Besides the reactions above, other channels for COF_2 formation are as follows:

$$CF_3 + O \rightarrow COF_2 + F, \quad 1.9\times10^{13}\,\mathrm{cm^3mol^{-1}s^{-1}} \tag{26}$$

$$CF_3 + NO_2 \rightarrow COF_2 + NOF, \quad 1.5\times10^{13}\,\mathrm{cm^3mol^{-1}s^{-1}} \tag{27}$$

$$COF + COF \rightarrow COF_2 + CO, \quad 8.0\times10^{12}\,\mathrm{cm^3mol^{-1}s^{-1}} \tag{28}$$

Under electrical discharge plasma, a part of COF_2 leads to carbon oxides such as CO_2 and CO (Herron, 1999; NIST, 1998)

$$COF_2 + O\left(^1D\right) \rightarrow CO_2 + F_2, \quad 1.3\times10^{13}\,\mathrm{cm^3mol^{-1}s^{-1}} \tag{29}$$

$$CO_2 + N\left(^2D\right) \rightarrow CO + NO, \quad 2.2\times10^{11}\,\mathrm{cm^3mol^{-1}s^{-1}} \tag{30}$$

Energetic electrons can also decompose CO_2 into CO by direct bond cleavage. The reaction pathways regarding CHF_3 destruction are described in Fig. 1.

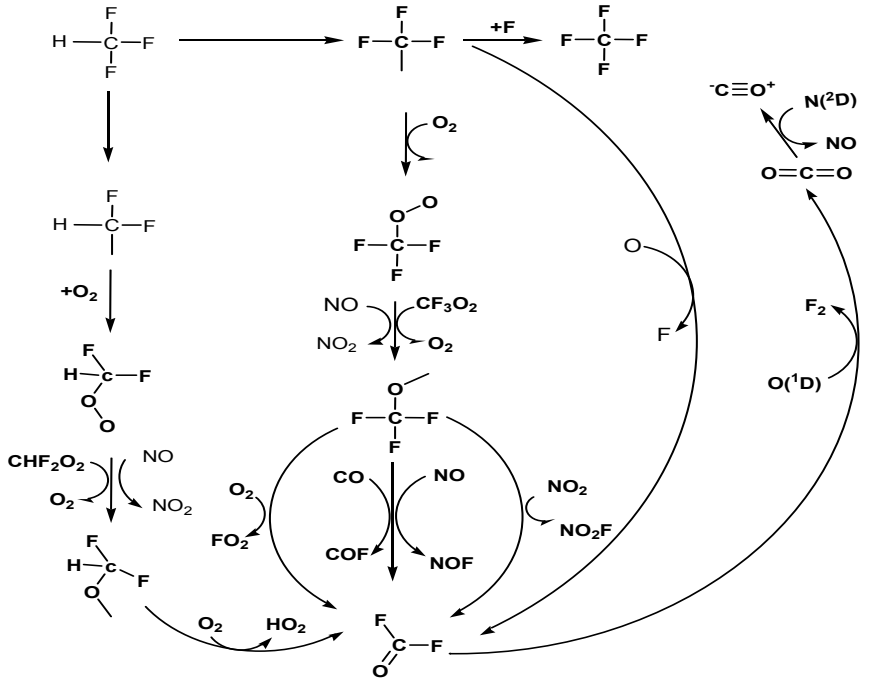

Fig. 1. Reaction pathways of CHF_3 destruction in the presence of N_2 and O_2

2.2.2 Hexafluoroethane

Hexafluoroethane (C_2F_6) is chemically very stable, which is attributed to the strength of C-F bond in it and the shielding effect of the fluorine atoms. Hence, the reactivity of C_2F_6 with the species generated by the plasma is extremely low. The most likely process for initiating the destruction of C_2F_6 is believed to be the dissociation by the energetic electrons generated by the plasma, which can be written as (Motlagh & Moore, 1998)

$$e + C_2F_6 \rightarrow CF_3 + CF_3 + e \tag{31}$$

$$e + C_2F_6 \rightarrow C_2F_5 + F + e \tag{32}$$

The bond dissociation energies of C-C and C-F are 3.6 and 5.1 eV, respectively, indicating that reaction (31) is superior to reaction (32). According to the mass spectrum of C_2F_6 that illustrates the cracking pattern, the most abundant fragment is CF_3, which supports that reaction (31) is the predominant electron impact dissociation process. Once CF_3 is produced somehow, succeeding reactions that convert CF_3 into carbon oxides can be explained by reactions (15)~(30). The plausible reaction pathways responsible for the destruction of C_2F_6, leading to the formation of CO and CO_2 are illustrated in Fig. 2 (Kim et al., 2010b). In the destruction of fluorinated compounds, the overall rate is determined by its initial

fragmentation by energetic electrons, i.e., electron impact dissociation process acts as the rate-determing step, and succeeding reactions are considered to be a lot faster.

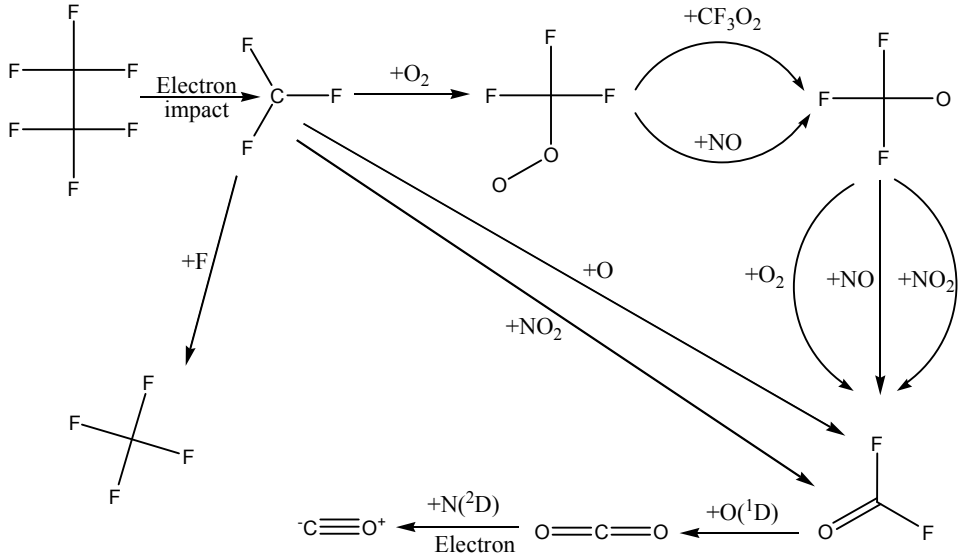

Fig. 2. Plausible reaction pathways responsible for the destruction of C_2F_6

2.2.3 1,1,1,2-tetrafluoroethane

In the same way, the destruction of $C_2H_2F_4$ can be explained with the bond dissociations followed by subsequent reactions leading to the formation of CO and CO_2. The initial destruction fragments of $C_2H_2F_4$ that are produced through collisions with energetic species such as electrons, $N(^2D)$ and N_2 ($A^3\Sigma_u^+$) include CH_2F, CF_3 and $CHF=CF_2$ (Mok et al., 2008):

$$C_2H_2F_4 + \text{energetic species} \rightarrow CH_2F + CF_3 \tag{33}$$

$$C_2H_2F_4 + \text{energetic species} \rightarrow CHF - CF_3 + H \rightarrow CHF = CF_2 + HF \tag{34}$$

Likewise, the fragments CH_2F and CF_3 further react with O, O_2 and O_3 to form carbon oxides, as described in reactions (15)~(30), which may be summarized as follows:

$$CF_3 \rightarrow CF_3O_2 \rightarrow CF_3O \rightarrow COF_2 \rightarrow CO,\ CO_2 \tag{35}$$

$$CH_2F \rightarrow CH_2FO_2 \rightarrow CH_2FO \rightarrow COF_2 \rightarrow CO,\ CO_2 \tag{36}$$

$$C_2H_2F_3 \rightarrow CHF = CF_2 \rightarrow HCOF\ +\ COF_2 \rightarrow CO,\ CO_2 \tag{37}$$

Being more specific about the reaction scheme (37), $CHF=CF_2$ formed by dehydrofluorination yields HCOF and COF_2 as a result of the addition of ozone to its double bond, which is typical in the reaction of alkene compounds with ozone:

$$CHF = CF_2 + O_3 \rightarrow HCOF + COF_2 + O,\ 1.1 \times 10^6\,cm^3 mol^{-1} s^{-1} \quad (38)$$

HCOF successively reacts as below to form COF_2

$$HCOF + F \rightarrow COF\ +\ HF,\ 5.3 \times 10^{11}\,cm^3 mol^{-1} s^{-1} \quad (39)$$

$$COF\ +\ F_2 \rightarrow COF_2,\qquad 2.7 \times 10^{10}\,cm^3 mol^{-1} s^{-1} \quad (40)$$

Even though the $C_2H_2F_4$ destruction can systematically be elucidated with the above reactions, there are many other possible reactions that simultaneously occur.

2.2.4 Sulfur hexafluoride

Finally, the electron impact dissociation of SF_6 can generally be expressed as (Nanjo & Ohyama, 2005)

$$SF_6 + e \rightarrow SF_x + (6-x)F,\ x \le 5 \quad (41)$$

Here, SF_x stands for intermediate decomposition products such as SF_5, SF_4, SF_3, etc, and they can be oxidized to form SO_2 and SO_2F_2. The reaction schemes involving oxygen have been proposed by different authors in order to explain the SO_2 and SO_2F_2 formation (Khairallah et al., 1994; Nanjo & Ohyama, 2005). The intermediate decomposition products of reaction (41) further react with atomic or molecular oxygen as follows:

$$SF_4 + O \rightarrow SOF_2 + 2F \quad (42)$$

$$SF_3 + O \rightarrow SOF_2 + F \quad (43)$$

$$SOF_2 + F \rightarrow SOF_3 \quad (44)$$

$$SOF_3 + O \rightarrow SO_2F_2 + F \quad (45)$$

$$SOF_2 + O \rightarrow SO_2F_2 \quad (46)$$

$$SF_3 + O_2 \rightarrow SO_2F_2 + F \quad (47)$$

$$SF_2 + O_2 \rightarrow SO_2F_2 \quad (48)$$

$$SO_2F_2 \rightarrow SO_2 + F_2 \quad (49)$$

These consecutive reactions lead to the formation of SO_2 and SO_2F_2.

3. Experimental section

DBD reactors can be constructed in many configurations, for instance, planar type using parallel-plate metal electrodes separated by a dielectric layer or cylindrical type consisting of two coaxial electrodes separated by a tubular dielectric layer between them. In this work, a cylindrical-type DBD reactor packed with catalyst pellets or dielectric beads was employed for the destruction of fluorinated compounds. The DBD nonthermal plasma

reactor of this work, referred to as plasma reactor, was made up of a ceramic tube serving as a dielectric barrier, a concentric stainless steel screw and a copper foil wrapping around the ceramic tube. The experimental details including apparatus, feed gas preparation, methods and analyses are described below.

3.1 Apparatus

Fig. 3 depicts the schematic diagram of the cylindrical plasma reactor of this work. The inner and outer diameter of the ceramic tube were 24.5 mm and 28 mm, where the stainless steel screw with a thickness of 6 mm was coaxially placed. In this reactor configuration, the stainless steel screw and the copper foil acted as the discharging and ground electrode, respectively. The effective reactor length for creating nonthermal plasma was about ~150 mm. The plasma reactor prepared as above was packed with 3-mm α-alumina beads (Sigma-Aldrich Co.), 3-mm glass beads (Sigmund-Lindner, Germany) or 3-mm zirconia beads (Daihan Scientific, Korea) to a volume of 127 cm^3. Unlike alumina widely used as a catalyst or a catalyst support, zirconia and glass beads have no catalytic activity, thus the contribution of the nonthermal plasma to the destruction of fluorinated compounds can solely be evaluated with these packing materials. The plasma reactor was also operated without any packing materials to contrast the results with those obtained in the presence of packing materials. So as to change the reactor temperature to a desired value, the plasma reactor was covered with a heating tape and the temperature was controlled by a proportional-integral-derivative (PID) controller. The reactor temperature was measured at the midpoint of the reactor wall by using a K-type thermocouple.

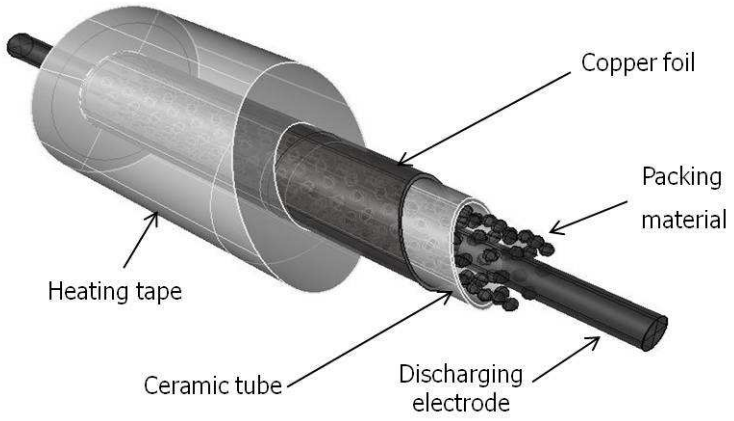

Fig. 3. Schematic diagram of the nonthermal plasma reactor

3.2 Methods

The schematic representation of the experimental setup is shown in Fig. 4. An alternating current (AC) high voltage power supply (operating frequency: 400 Hz) was used to energize the plasma reactor. The voltage applied to the discharging electrode of the plasma reactor was varied in the range of 7~16 kV (rms value) to change the electrical power delivered to the plasma reactor. The fluorinated compounds dealt with in this work were CHF_3, $C_2H_2F_4$, SF_6 and C_2F_6. The behavior of destruction of these compounds was separately examined one

by one. The feed gas consisted of three gases, i.e., a fluorinated compound, nitrogen and oxygen, whose flow rates were regulated by mass flow controllers (MKS Instruments, Inc., USA). The concentration of the fluorinated compound at the reactor inlet was typically at 2,000 ppm (parts per million, volumetric). The overall flow rate of the feed gas was 1.0 L min^{-1} or 60 L h^{-1} on the basis of room temperature. The reactor temperature was changed up to 500°C by applying heat to the reactor using a heating tape. The simulated exhaust gas processed in the plasma reactor was directed to the Fourier transform infrared (FTIR) Spectrometer (Bruker IFS 66/S, Germany) for analyzing fluorinated compounds and destruction products. The fluorinated compounds and byproducts were assigned in the spectra and the measured absorbance of each compound was converted into concentration units. The decomposition efficiency was defined as $100 \times (C_0\text{-}C)/C_0$, where C_0 and C are the concentrations at the inlet and outlet of the reactor, respectively. The electrical power (input power) was measured by a digital power meter (Model WT200, Yokogawa, Japan) and the voltage was monitored using a digital oscilloscope (TDS 3032, Tektronix, USA) equipped with a 1000 : 1 high voltage probe (P6015, Tektronix, USA).

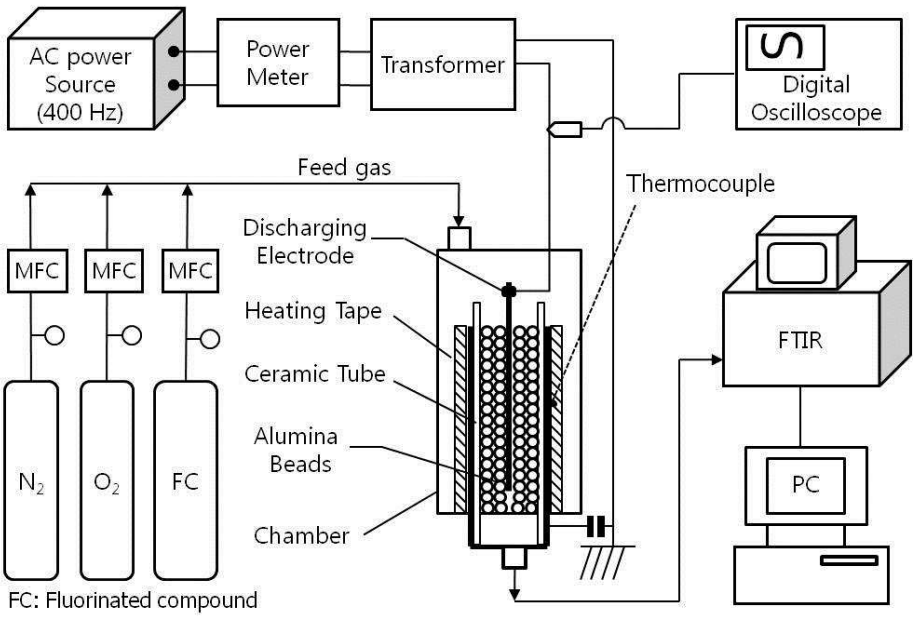

Fig. 4. Schematic of the experimental setup for destroying fluorinated compounds

Discharge power that is actually consumed in the plasma reactor was determined by using the so-called Lissajous charge-voltage curve (Rosocha, 2005). The Lissajous curve was obtained by measuring the voltages across the electrodes of the plasma reactor and across the capacitor (0.43 μF) connected to the plasma reactor in series. The voltage across the capacitor multiplied by its capacitance corresponds to the charge, which is, in principle, equal to the charge accumulated on the electrodes of the plasma reactor because the

capacitor and the plasma reactor are a series circuit. Fig. 5 (a) shows example waveforms of the voltage applied to the plasma reactor and the charge deposited, and Fig. 5 (b) shows the Lissajous curve for the voltage versus the charge. The energy per cycle consumed in the plasma reactor is equal to the enclosed area, and the discharge power can be calculated by multiplying the energy per cycle by the operating frequency (400 Hz).

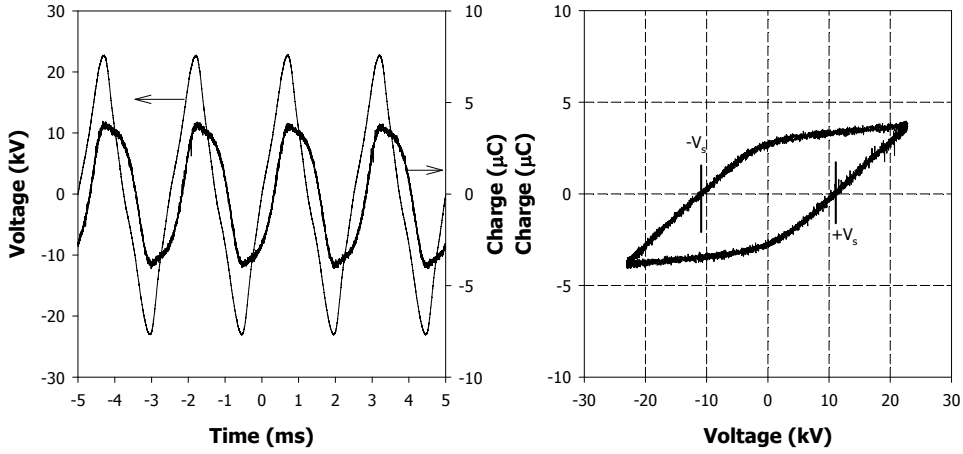

Fig. 5. (a) Waveforms of the voltage applied to the plasma reactor and the charge deposited and (b) the corresponding Lissajous figure

4. Results and discussion

4.1 Discharge power

The performance of the plasma reactor is a strong function of temperature, especially when it is packed with catalyst pellets, and accordingly, it is necessary to recognize the relationship between the reactor temperature and the discharge power. The DBD plasma is characterized by numerous short lifetime microdischarges, which are generated when the applied voltage exceeds the breakdown voltage of the gas between the electrodes. The microdischarges form conduction paths between the electrodes, and self-extinguish as the charge accumulated on the dielectric reduces the local electric field. Fig. 6 shows the dependence of the discharge power on the reactor temperature and the type of packing materials (alumina, zirconia and glass beads), when the input power was 60~100 W. The plasma reactor can electrically be treated as a capacitor, and the discharge power was measured by using the Lissajous curve (Rosocha, 2005). As presented in Fig. 6, regardless of the packing material used, the temperature-discharge power relationships were similar to one another. Regarding the temperature effect for 60 W and 80 W input power, the discharge power gradually increased with increasing the temperature up to 200°C, and then stabilized with further increase in the temperature above 200°C. As well known, gaseous molecules can be more easily ionized at higher temperatures, which results in increasing the discharge power. For 100 W input power, the temperature effect on the discharge power was not significant. The efficiency of power transfer, defined as the ratio of discharge power to input power, was calculated to be about 70%.

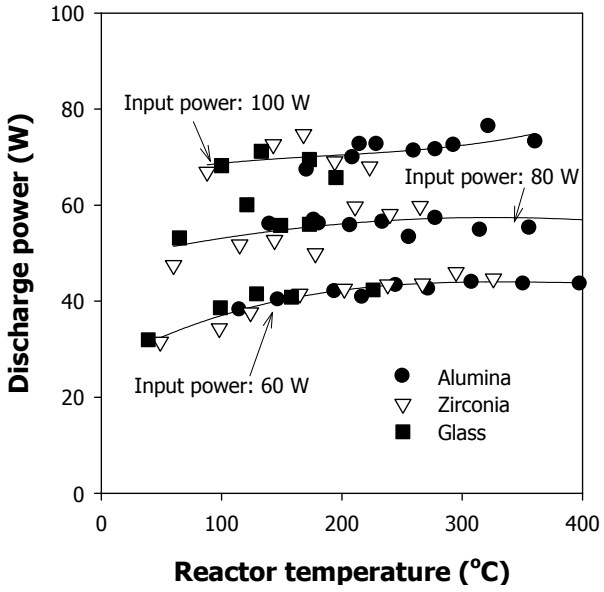

Fig. 6. Dependence of the discharge power on the reactor temperature and the type of packing material

4.2 Effect of reactor temperature

The plasma reactor packed with alumina beads showed different behaviors according to the reactor temperatures. Below a certain threshold temperature, the destruction efficiency slowly increased with increasing the reactor temperature, while on the other hand there was a steep increase in the destruction efficiency as the reactor temperature was further increased beyond the threshold temperature (Kim et al., 2010c; Kim & Mok, 2010; Kim and Mok, 2011). The threshold temperature was found to vary with the fluorinated compounds investigated. Details are given below.

The effect of the reactor temperature on the destruction of CHF_3 is shown in Fig. 7. The input power was fixed at 80 W (discharge power: ~56 W) ove a reactor temperatures range up to 300°C. The destruction efficiency was observed to increase with increasing the reactor temperature, implying that the reactions responsible for the CHF_3 destruction are advantageous at elevated temperatures. In addition, the increase in the discharge power with increasing the temperature (see Fig. 6) may partly explain why higher destruction efficiency was observed at higher temperature. Meanwhile, at temperatures below 150°C where the catalytic activity may be neglected, the difference in the destruction efficiency between the alumina and glass beads was inconsiderable. On the other hand, the difference became pronounced when the reactor temperature was further increased over 150°C, because the catalytic destruction played an important role in this temperature region and the plasma possibly assisted the catalytic reactions.

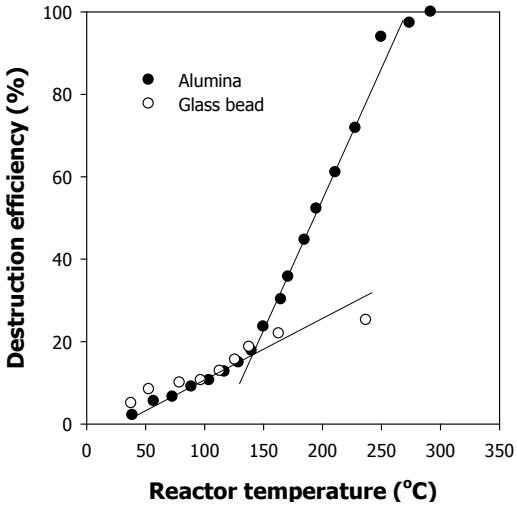

Fig. 7. Variations of the HFC decomposition efficiency as a function of reactor temperature (CHF_3: 2,000 ppm; O_2: 1.0%(v/v); input power: 80 W)

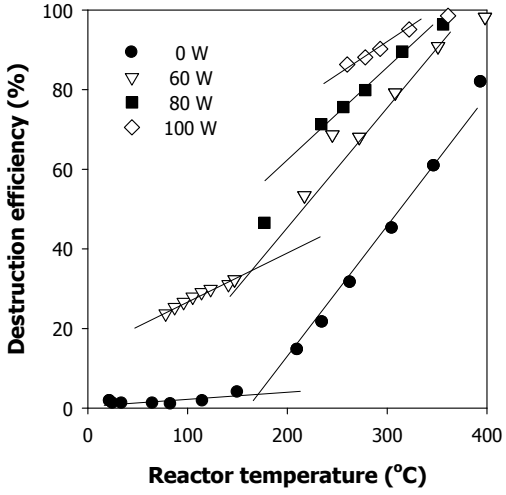

Fig. 8. Comparison of $C_2H_2F_4$ destruction efficiencies between catalysis alone and plasma-catalysis over a temperature range up to 400°C ($C_2H_2F_4$: 2,000 ppm; O_2: 2.0%(v/v)

Fig. 8 presents a comparison of $C_2H_2F_4$ destruction efficiencies between without plasma and with plasma over a temperature range up to 400°C at input powers of 60~100 W (discharge power: 42~60 W), which was obtained with alumina beads as the packing material. In this

figure, the catalysis-alone case corresponding to the results obtained at 0 W indicates that the alumina catalyst was thermally activated without applying high voltage to the reactor, and the plasma-catalysis (60~100 W) represents that both thermal and plasma activation of the catalyst worked upon the $C_2H_2F_4$ destruction.

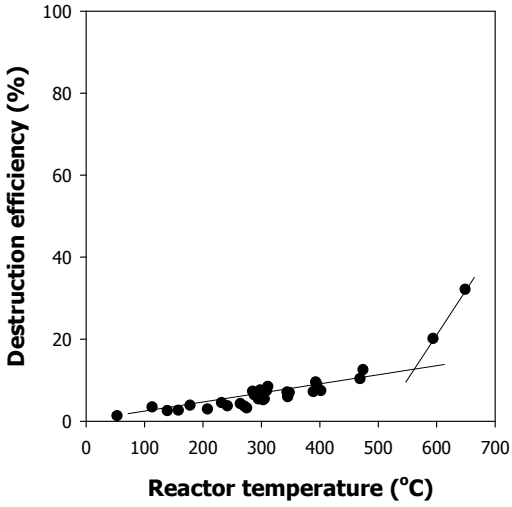

Fig. 9. Effect of reactor temperature on the destruction of C_2F_6 (C_2F_6: 2,000 ppm; O_2: 2.0%(v/v); input power: 100 W)

As can be seen in Fig. 8, the catalyst alone started destroying the fluorinated compound from about 150°C, exhibiting negligible destruction efficiency at temperatures below 150°C. When the reactor temperature was gradually increased from 150°C to 400°C at 60 W, the destruction efficiency proportionally increased, reaching 80% at 400°C. In the case of the plasma plus catalysis, it is apparent that the $C_2H_2F_4$ destruction can be divided into two different regions by the steepness of the temperature-destruction efficiency relationship. In the lower temperature region below 150°C, the $C_2H_2F_4$ destruction efficiency slowly increased with increasing the reactor temperature, while in the higher temperature region the destruction efficiency rapidly increased with increasing the reactor temperature, approaching complete destruction at around 400°C. The lower temperature region where the catalyst has no activity is understood to have been dominated by gas-phase reactions resulting from various actions of the plasma. On the other hand, above 150°C, both the plasma and the catalysis must have affected the $C_2H_2F_4$ destruction, thereby leading to a steeper increase in the destruction efficiency. The threshold temperatures were around 150°C for $C_2H_2F_4$, but as shown in Fig. 9, the threshold temperature for C_2F_6 destruction was found to be much higher around 600°C, despite similar molecular structure to one another. This result can be attributed to the fact that C_2F_6 does not have relatively weak C-H bonds, i.e., since C_2F_6 consists only of strong C-F bonds, the high bond dissociation potential and and the shielding effect of the fluorine atoms make the reactivity of C_2F_6 extremely low.

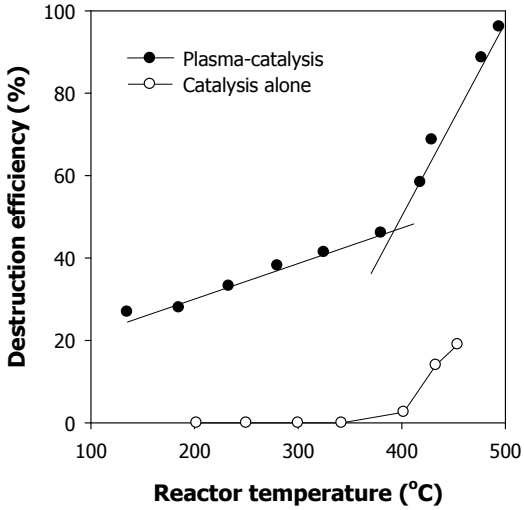

Fig. 10. Effect of reactor temperature on the destruction of SF_6 (SF_6: 2,000 ppm; O_2: 2.0%(v/v); input power: 100 W)

Fig. 10 shows the effect of the reactor temperature on the destruction of SF_6. It can be seen that the SF_6 destruction efficiency increased slowly from 27% to 46% with increasing the reactor temperature from 135°C to 380°C, and then abruptly increased with further increasing the reactor temperature, reaching 96% destruction efficiency at 495°C. From this result, the destruction of SF_6 in the plasma-catalysis combined system can be divided into two different regions, according to the reactor temperature. The threshold temperature for the nonthermal plasma-assisted catalysis is seen to be around 400°C. Below 400°C is the region of no catalytic activity, and above 400°C is the region dominated by the nonthermal plasma-assisted catalysis. In the low temperature region below 400°C, the slow increase in the destruction efficiency with increasing the reactor temperature can be explained by the decrease in the gas density. As the gas density decreases, electrons generated in the plasma reactor can be accelerated more efficiently to destroy SF_6 molecules because the mean free path correspondingly increases. In the high temperature region above 400°C, there was a precipitous increase in the destruction efficiency. It is the region dominated by the nonthermal plasma-assisted catalysis, where processing the simulated exhaust gas produced over 95% decomposition efficiency at temperatures higher than 490°C, compared with 27~46% in the low temperature region. In Fig. 10, the data resulting from the catalysis alone are also presented. In the absence of plasma, the catalyst exhibited no SF_6 decomposition efficiency at temperatures below 400°C. It was observed that the catalyst began decomposing SF_6 from about 400°C, which is in agreement with the threshold temperature mentioned above. Consequently, it can be said that the temperature starting to show an abrupt increase in the decomposition efficiency is the one for the catalyst to begin exhibiting its activity. Once the catalyst begins exhibiting its activity, the nonthermal plasma can remarkably enhance the decomposition, as shown in Fig. 10. From such a large enhancement in the destruction efficiency in the presence of the nonthermal plasma, it is apparent that the plasma-assisted catalysis is a very effective way to improve the catalytic activity at relatively low temperatures.

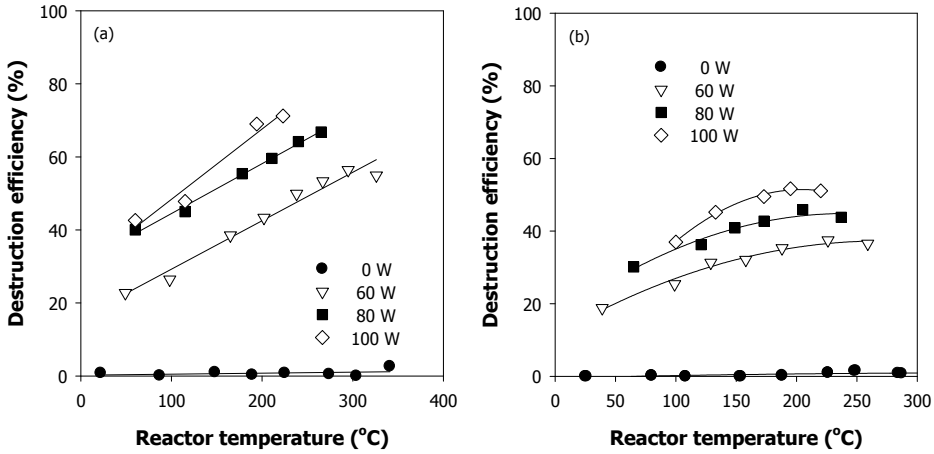

Fig. 11. Comparison of $C_2H_2F_4$ destruction efficiencies between (a) zirconia and (b) glass beads ($C_2H_2F_4$: 2,000 ppm; O_2: 2.0%(v/v))

4.3 Effect of packing material type

The destruction of fluorinated compounds by the plasma can strongly depend on the type of packing material, especially at high temperatures that the contribution of catalysis can be significant. In Fig. 11, a comparison between zirconia and glass beads was made under the same input power conditions as a function of the reactor temperature. The results obtained with alumina are presented in Fig. 8 above. It should be noted that zirconia and glass beads have negligible catalytic activity for the destruction of fluorinated compounds. In all cases, increasing the reactor temperature enhanced the destruction efficiency. The increase in the destruction efficiency with increasing the temperature can be attributed to the decrease in the gas density. Namely, the decrease in the gas density increases the mean free path of electrons, which in turn accelerates electrons more efficiently to increase the generation of reactive species and the electron-impact dissociation of $C_2H_2F_4$ molecules. Meanwhile, as observed in Fig. 8 and Fig. 11, the difference in the destruction efficiencies between the three types of packing materials was inconsiderable at lower temperature region. Such a phenomenon was also shown in the destruction of CHF_3 as described in Fig. 7. However, at temperatures above 150°C, the difference in the destruction efficiencies became pronounced, obviously because the catalytic action of alumina significantly contributed to the $C_2H_2F_4$ destruction. Despite both having negligible catalytic activity, the behavior of $C_2H_2F_4$ destruction with zirconia beads was different from that with glass beads, which may be explained by the difference in their dielectric constants. The discharge characteristics of a packed-bed type plasma reactor largely depend on the dielectric constant of packing material, and larger dielectric constant is generally more advantageous to the performance of plasma reactor. The dielectric constants of zirconia and silica glass are 15~22 and 3.8, respectively, and it is reasonable that the reactor packed with zirconia beads produced higher destruction efficiency than that with glass beads.

Fig. 12 presents the FTIR spectra of the gas processed in the plasma reactor, which were obtained with alumina and zirconia as the packing materials (Mok & Kim, 2011). With

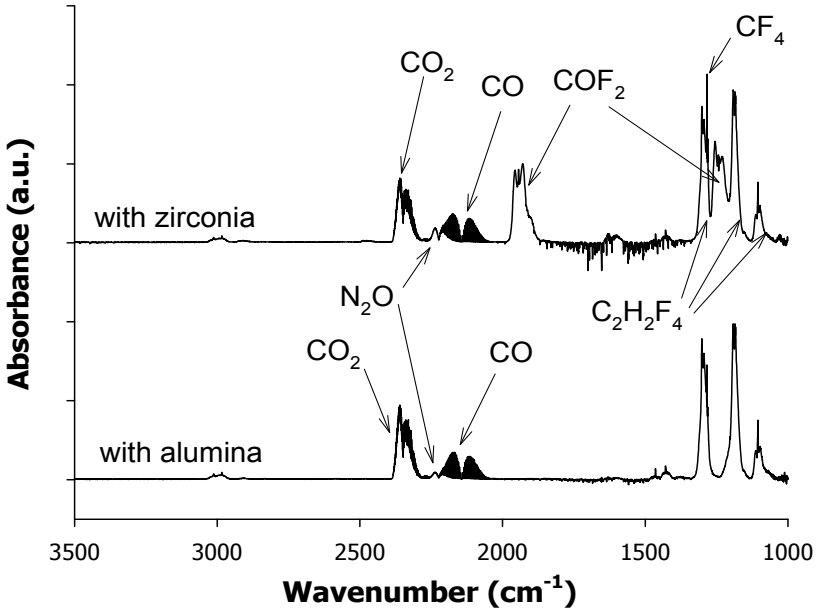

Fig. 12. FTIR spectra of the gas processed in the plasma reactor ($C_2H_2F_4$: 2,000 ppm; O_2: 2.0%(v/v); input power: 60 W)

zirconia, the carbon-containing byproducts identified included CO_2, CO, carbonyl fluoride (COF_2) and carbon tetrafluoride (CF_4). According to the reactions schemes explained above, COF_2 serves as a key intermediate compound to convert fluorinated compounds into CO and CO_2. Different from the result obtained with zirconia, however, COF_2 was disappeared in the FTIR spectrum when alumina was used as the packing material. It has been shown above that alumina exhibits it catalytic activity for destroying $C_2H_2F_4$, starting at around 150°C. Besides such a capability for destroying $C_2H_2F_4$, the FTIR spectrum suggests that alumina can also move the process towards the total oxidation, oxidizing COF_2 to CO and CO_2. Since COF_2 is a highly toxic compound, the use of alumina is more advantageous.

Figs. 13 (a) and (b) show the concentrations of the carbon-containing destruction products that were obtained with alumina and zirconia as the packing material, respectively. Although data are not shown, nitrous oxide (N_2O) was also identified in the effluent gas stream. The formation of N_2O is common in plasma processing of air-like gases containing both N_2 and O_2 (Fitzsimmons et al., 2000; Ricketts et al., 2004; Harling et al., 2005). Properly, the amounts of destruction products were more in the presence of alumina than zirconia, because of higher destruction efficiency. In both cases of packing materials, the abundant destruction products were CO_2 and CO. The concentrations of CO_2 and CO tended to increase with increasing the reactor temperature. Even though the amounts were small, the plasma reactor packed with zirconia beads produced COF_2 and CF_4. The main reaction for the formation of CF_4 is the recombination of CF_3 and F.

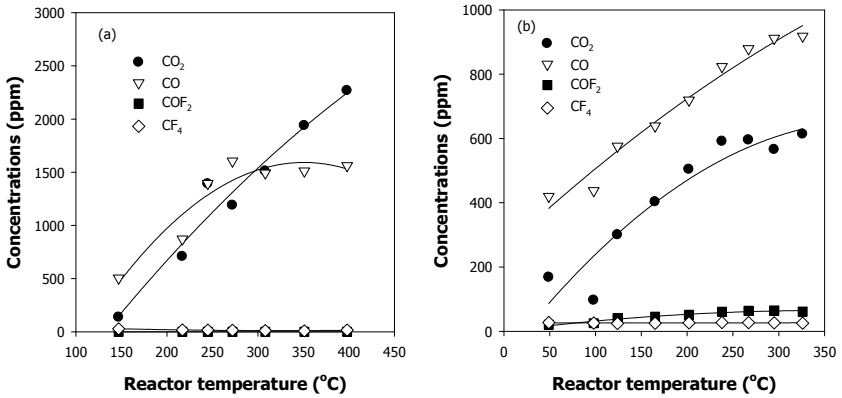

Fig. 13. Byproducts distribution: (a) with alumina and (b) with zirconia ($C_2H_2F_4$: 2,000 ppm; O_2: 2.0%(v/v); input power: 60 W)

4.4 Synergistic effect of plasma-catalysis

In Fig. 14, the destruction efficiencies obtained with the nonthermal plasma-alone case, the catalyst-alone case and the plasma-catalyst case are compared for input powers of 60 W and 80 W. In the case of "the plasma alone", the reactor was packed with the glass beads, because the glass beads do not have any catalytic activity for destroying fluorinated compounds. The cases of "the plasma-catalyst" and "the catalyst alone" represent the catalytic CHF_3 decomposition performed with and without the plasma, respectively. In Fig. 14, an interesting aspect of the plasma-catalyst is the so-called synergistic effect. At an input power of 80 W, the plasma-alone case decomposed about 24% and 28% of CHF_3 at 200°C and 250°C, respectively. The respective destruction efficiencies obtained by the catalyst-alone case at the corresponding temperatures were 10% and 33%. The arithmetic sum of

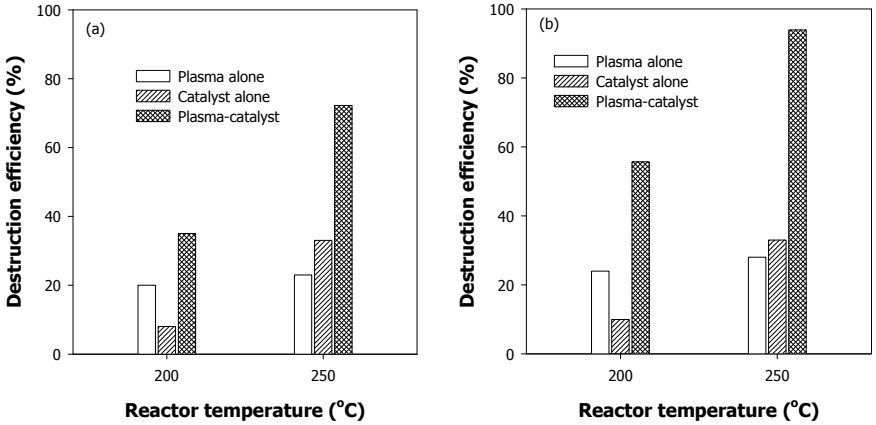

Fig. 14. Comparison of decomposition efficiency between the plasma alone, the catalyst alone and the plasma-catalyst combination at input powers of (a) 60 W and (b) 80 W (CHF_3: 2,000 ppm; O_2: 1.0%(v/v)).

the plasma and catalyst decompositions individually adds to 34% and 61% at 200°C and 250°C, respectively. However, in the case of the plasma-catalyst, the destruction efficiencies at the respective temperatures were 56% and 94%, clearly showing that there was some synergy. The synergistic effect implies that the plasma can provide some additional activation of the alumina catalyst (Kim et al., 2005; Kim et al., 2010c). In this context, it would be advisable to combine the plasma and the catalyst rather than use them separately. When the input power was 60 W, the destruction efficiencies obtained by the plasma-alone case were 20% and 23% at 200°C and 250°C, and those obtained by the plasma-catalyst were 35% and 72 %, respectively. The sum of the destruction efficiencies individually obtained by the plasma and catalyst is 30% at 200°C and 56% at 250°C, which are smaller values when compared to 35% and 72 % obtained by the combination of plasma and catalyst at identical temperatures.

In the destruction of fluorinated compounds, the overall destruction rate is determined by the electron impact dissociation, and succeeding reactions for oxidizing the destruction fragments are much faster. The enhancement of the destruction efficiency with the plasma-catalyst case may be explained by the acceleration of the rate-determining step. The C-F bond strength for a gaseous fluorinated compound is 5.1 eV, but it gets weak when adsorbed on the catalyst surface. As a result, the energetic electrons generated by the plasma can more easily break the C-F bond of the adsorbed molecule through direct electron impact, speeding up the rate-determining step.

4.5 Effect of electric power

In Fig. 15, the effect of the electrical power on the destruction of CHF_3 at different temperatures in the range of 150~250°C. The input power was changed up to 100 W. The discharge power was about 70% of the input power. In this figure, the results at 0 W that the CHF_3 destruction efficiencies obtained with the catalysis alone. As can be seen in Fig. 15 (a), the alumina exhibited negligible catalytic destruction efficiency below 150°C, but its catalytic activity was gradually enhanced with increasing the reactor temperature. On the contrary, the reactor packed with the glass beads did not decompose CHF_3 at all temperatures explored. Moreover, the effect of the electric power on the destruction was even more significant for

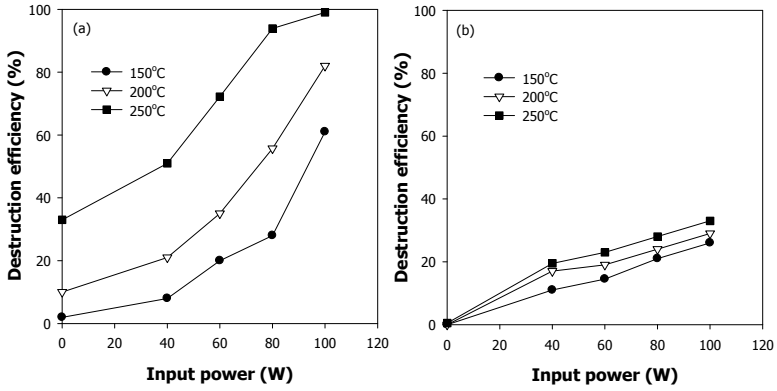

Fig. 15. Effect of the electric power on the decomposition of CHF_3 (a) with alumina and (b) with glass beads (CHF_3: 2,000 ppm; O_2: 1.0%(v/v))

alumina beads than for glass beads, obviously because various actions of the plasma assisted catalytic reactions. The destruction efficiency versus the input power for alumina-packed case (Fig. 15 (a)) showed an exponential growth whereas that for glass-packed case (Fig. 15 (b)) showed a linear increase. With glass beads, only gas-phase reactions induced by the plasma are responsible for the CHF_3 destruction. As shown in Fig. 15 (a), the higher the reactor temperature, the less the input power required to destroy CHF_3, due to the improved catalytic activity. When the reactor temperature was 250°C, the destruction efficiency with the alumina approached 100% at an input power of 100 W. This is neary three times higher destruction efficiency, when compared to a little more than 30% in the presence of glass beads.

5. Conclusions

The destruction of several fluorinated compounds such as trifluoromethane (CHF_3), sulfur hexafluoride (SF_6), 1,1,1,2-tetrafluoroethane ($C_2H_2F_4$) and hexafluoroethane (C_2F_6) was investigated in the plasma reactor packed with alumina, zirconia or glass beads. This work was concentrated on the effects of reactor temperature and electric power, and the conclusions drawn are as follows. Operating the plasma reactor at elevated temperatures was advantageous, owing to increased rates of destruction reactions. Particularly, the favorable effect of the elevated temperature on the destruction was remarkable in the presence of alumina, because it acted as a catalyst.

From several sets of catalyst-alone experiments, it was found that the threshold temperature from which the destruction efficiency began rapidly rising corresponds to the minimum activation temperature of the alumina catalyst. The threshold temperatures were around 150°C for CHF_3 and $C_2H_2F_4$, around 400°C for SF_6, and around 600°C for C_2F_6. On the contrary, with zirconia or glass beads as the packing material, the temperature dependence of the destruction efficiency did not show such a threshold, indicating that the destruction was mainly caused by gas-phase reactions. Even though the temperature dependence on the destruction with zirconia or glass beads was not as remarkable as with alumina beads, the reactor packed with zirconia beads having larger dielectric constant produced higher destruction efficiency than that with glass beads.

This study has shown that the combination of plasma and catalyst may be an effective method to destroy fluorinated compounds. The plasma-catalyst combination showed higher destruction efficiency than the sum of those individually obtained by the plasma and the catalyst. This synergistic effect indicates that the nonthermal plasma created in the catalytic reactor can provide some additional activation of the catalyst.

6. Acknowledgment

The author would like to thank members of the Jeju National University Plasma Applications Laboratory whose work is referred to this article: D. H. Kim, S. B. Lee, J. H. Oh, E. J. Jwa, and M. Gandhi. Financial support from the National Research Foundation of Korea (Grant number 2010-0021672) is greatly acknowledged.

7. References

Barker, J. R. (1995). *Progress and Problems in Atmospheric Chemistry*, World Scientific, ISBN 981-02-1868-0, London, UK

Bickle, G.M.; Suzuki, T. & Mitarai, Y. (1994). Catalytic Destruction of Chlorofluorocarbons and Toxic Chlorinated Hydrocarbons. *Applied Catalysis B: Environmental*, Vol. 4, (1994), pp. 141-153, ISSN 0926-3373

Chang, M.B.; Balbach, J.H.; Rood, M.J. & Kushner, M.J. (1991). Removal of SO_2 from Gas Streams Using a Dielectric Barrier Discharge and Combined Plasma Photolysis. *Journal of Applied Physics*, Vol.69, No. 8, (April 1991), pp. 4409-4417, ISSN 0021-8979

Futamura, S. & Yamamoto, T. (1997). Byproducts Identification and Mechanism Determination in Plasma Chemical Decomposition of Trichloroethylene. *IEEE Transactions on Industry Applications*, Vol. 33, No. 2, (March & April 1997), pp. 447-453, ISSN 0093-9994

Fitzsimmons, C.; Ismail, F.; Whitehead, J.C. & Wilman, J.J. (2000). The Chemistry of Dichloromethane Destruction in Atmospheric-Pressure Gas Streams by a Dielectric Packed-Bed Plasma Reactor. *Journal of Physical Chemistry A*, Vol. 104, (2000), pp. 6032-6038, ISSN 1089-5639

Föglein, K.A.; Szabó, P.T.; Babievskaya, I.Z. & Szépvölgyi, J. (2005). Comparative Study on the Decomposition of Chloroform in Thermal and Cold Plasma. *Plasma Chemistry and Plasma Processing*, Vol. 25, No. 3, (2005), pp. 289-302, ISSN 0272-4324

Futamura, S. & Yamamoto, T. (1997). Byproducts Identification and Mechanism Determination in Plasma Chemical Decomposition of Trichloroethylene. *IEEE Transactions on Industry Applications*, Vol. 33, No. 2, (March & April 1997), pp. 447-453, ISSN 0093-9994Harling, A.; Whitehead, J.C. & Zhang, K. (2005). NO_x Formation in the Plasma Treatment of Halomethane. *Journal of Physical Chemistry A*, Vol. 109, (2005), pp. 11255-11260, ISSN 1089-5639

Herron, J. T. (1999). Evaluated Chemical Kinetics Data for Reactions of $N(^2D)$, $N(^2P)$, and $N_2(A^3\Sigma_u^+)$ in the Gas Phase. *Journal of Physical and Chemical Reference Data*, Vol.28, No.5, (1999), pp. 1453-1483, ISSN 0047-2689

Kim, D.H.; Mok, Y.S.; Lee, S.B. & Shin, S.M. (2010a). Nonthermal Plasma Destruction of Trifluoromethane Using a Dielectric-Packed Bed Reactor. Jornal of Advanced Oxidation Technologies, Vol. 13, (2010), pp. 36-42, ISSN 1203-8407

Kim, D.H.; Mok, Y.S.; Lee, S.B. & Shin, S.M. (2010b). Destruction of Hexafluoroethane in a Dielectric-Packed Bed Plasma Reactor. *Journal of Zhejiang University-Science A*, Vol.11, No.7, (July 2010), pp. 538-544, ISSN 1673-565X

Kim, D.H.; Mok, Y.S. & Lee, S.B. (2010c). Effect of Temperature on the Decomposition of Trifluoromethane in a Dielectric Barrier Discharge Reactor. *Thin Solid Films*, (November 2010) doi:10.1016/j.tsf.2010.11.060, ISSN 0040-6090

Kim, H.H. Ogata, A. & Futamura, S. (2005). Atmospheric Plasma-Driven Catalysis for the Low Temperature Decomposition of Dilute Aromatic Compounds. *Journal of Physics D: Applied Physics*, Vol. 38, No.8, (2005), pp. 1292-1300, ISSN 0022-3727

Kim, D.H. & Mok, Y.S. (2010). Decomposition of Sulfur Hexafluoride by Using Nonthermal Plasma-Assisted Catalytic Process, *3rd Euro-Asian Pulsed Power Conference & 18th International Conference on High-Power Particle Beams*, Jeju, Korea, October 10-14, 2010

Kim, D.H. & Mok, Y.S. (2011). Destruction of Tetrafluoroethane with Atmospheric Nonthermal Plasma Created in Dielectric-Packed Bed Reactors, *I5th International Congress of Chemistry and Environment* (Organizer: Research Journal of Chemistry and Environment, India), Negeri Senbilan, Malaysia, May 27-29, 2011

Kim, H.H. Ogata, A. & Futamura, S. (2005). Atmospheric Plasma-Driven Catalysis for the Low Temperature Decomposition of Dilute Aromatic Compounds. *Journal of Physics D: Applied Physics*, Vol. 38, No.8, (2005), pp. 1292-1300, ISSN 0022-3727.

Khairallah, Y.; Khonsari-Arefi, F. & Amouroux, J. (1994). Decomposition of Gaseous Dielectrics (CF_4, SF_6) by a Non-Equilibrium Plasma. Mechanisms, Kinetics, Mass Spectrometric Studies and Interactions with Polymeric Targets. *Pure and Applied Chemistry*, Vol.66, No.6, (1994), pp. 1353-1362, ISSN 1365-3075

Kuroki, T.; Mine, J.; Okubo, M.; Yamamoto, T. & Saeki, N. (2005). CF_4 Decomposition Using Inductively Coupled Plasma: Effect of Power Frequency. *IEEE Transactions on Industry Applications*, Vol. 41, No. 1, (January & February 2005), pp. 215-220, ISSN 0093-9994

Lee, M.C. & Choi, W. (2004). Development of Thermochemical Destruction Method of Perfluorocarbons (PFCs). *Journal of Industrial and Engineering Chemistry*, Vol. 10, No. 1, (2004), pp. 107-114, ISSN 1226-086X

Li, J.; Sun W.; Pashaie, B. & Dhali, S. K. (1995). Streamer Discharges Simulation in Flue Gas. *IEEE Transactions on Plasma Science*, Vol.23, No.4, (August 1995), pp. 672-678, ISSN 0093-3813

Mizeraczyk, J.; Jasinski, M. & Zakrzewski, Z. (2005). Hazardous Gas Treatment Using Atmospheric Pressure Microwave Discharges. *Plasma Physics and Controlled Fusion*, Vol. 47, (2005), pp. B589–B602, ISSN 1361-6587

Mok, Y.S.; Ham, S.W. & Nam, I.-S. (1998). Mathematical Analysis of Positive Pulsed Corona Discharge Process Employed for Removal of Nitrogen Oxides. *IEEE Transactions on Plasma Science*, Vol. 26, No. 5, (October 1998), pp. 1566-1574, ISSN 0093-3813

Mok, Y.S.; Demidyuk, V. & Whitehead, J.C. (2008). Decomposition of Hydrofluorocarbons in a Dielectric-Packed Plasma Reactor. *Journal of Physical Chemistry A*, Vol. 112, (2008), pp. 6586-6591, ISSN 1089-5639

Motlagh, S. & Moore, J.H. (1998). Cross Sections for Radicals from Electron Impact on Methane and Fluoroalkanes. *Journal of Chemical Physics*, Vol.109, No.2, (July 1998), pp. 432-438, ISSN 0021-9606

Nanjo, Y. & Ohyama, R. (2005). An Experimental Study on Vacuum-Ultraviolet Photochemical Reaction to Non-Thermal Plasma Oxidized SF_6 Gases, *IEEE Conference on Electrical Insulation and Dielectric Phenomena*, pp. 689-692, Nashville, Tennessee, USA, October 16-19, 2005

National Institute of Standards and Technology (NIST) Chemical Kinetics Database: Version 2Q98, 1998

Ogata, A.; Kim, H.H.; Futamura, S.; Kushiyama, S. & Mizuno, K. (2004). Effects of Catalysts and Additives on Fluorocarbon Removal with Surface Discharge Plasma. *Applied Catalysis B: Environmental*, Vol. 53, (2004), pp. 175-180, ISSN 0926-3373

Piper, L.G.; Marinelli, W.J.; Rawlins, W.T. & Green, B.D. (1985). The Excitation of IF($B^3\Pi_{0+}$) by $N_2(A^3\Sigma_u^+)$. *Journal of Chemical Physics*, Vol. 83, No. 11, (December 1985), pp. 5602-5609, ISSN 0021-9606

Ricketts, C.L.; Wallis, A.E.; Whitehead, J.C. & Zhang, K. (2004). A Mechanism for the Destruction of CFC-12 in a Nonthermal, Atmospheric Pressure Plasma. *Journal of Physical Chemistry A*, Vol. 108, (2004), pp. 8341-8345, ISSN 1089-5639

Rosocha, L.A. (2005). *IEEE Transactions on Plasma Science*, Vol.33, No.1, (February 2005), pp. 129-137, ISSN 0093-3813

Tao, W.; Golde, M.F. & Ho, G.H. (1992). Experimental Study of the Reactions of $N_2(A\,^3\Sigma^+_u)$ with CH_3CN and HCN: The Effect of Vibrational Energy in $N_2(A)$. *Journal of Chemical Physics*, Vol.96, No. 1, (January 1992), pp. 356-366, ISSN 0021-9606

The Intergovernmental Panel on Climate Change (IPCC) Third Assessment Report: Climate Change. (2001)

Planet Earth 2011 - Global Warming Challenges and Opportunities for Policy and Practice

Edited by Prof. Elias Carayannis

ISBN 978-953-307-733-8
Hard cover, 646 pages
Publisher InTech
Published online 30, September, 2011
Published in print edition September, 2011

The failure of the UN climate change summit in Copenhagen in December 2009 to effectively reach a global agreement on emission reduction targets, led many within the developing world to view this as a reversal of the Kyoto Protocol and an attempt by the developed nations to shirk out of their responsibility for climate change. The issue of global warming has been at the top of the political agenda for a number of years and has become even more pressing with the rapid industrialization taking place in China and India. This book looks at the effects of climate change throughout different regions of the world and discusses to what extent cleantech and environmental initiatives such as the destruction of fluorinated greenhouse gases, biofuels, and the role of plant breeding and biotechnology. The book concludes with an insight into the socio-religious impact that global warming has, citing Christianity and Islam.

INTECH
open science | open minds

InTech Europe
University Campus STeP Ri
Slavka Krautzeka 83/A
51000 Rijeka, Croatia
Phone: +385 (51) 770 447
Fax: +385 (51) 686 166
www.intechopen.com

InTech China
Unit 405, Office Block, Hotel Equatorial Shanghai
No.65, Yan An Road (West), Shanghai, 200040, China
中国上海市延安西路65号上海国际贵都大饭店办公楼405单元
Phone: +86-21-62489820
Fax: +86-21-62489821